INTERACTION OF MEDIUM-ENERGY (10 – 100 keV) ATOMIC PARTICLES WITH SOLIDS (ENERGY SPECTRA OF SECONDARY IONS)

B. V. PANIN

Submitted to JETP editor September 29, 1960

The energy spectra are reported for secondary ions from molybdenum and beryllium targets, bombarded with the 7.5 – 80 keV ions H_1^+, H_2^+, He^+, N_1^+, N_2^+, O_1^+, O_2^+, CO^+, Ar^+, Ar^{2+}. Calculations of the detailed structure of these spectra are given. The validity of the classical mechanics description of the mechanism of ion emission is confirmed.

REQUIREMENTS of many branches of science and technology have stimulated studies of the phenomena occurring during bombardment of solid surfaces with various medium-energy atoms or ions. Investigations of the energy spectra of secondary ions produced by such bombardment yield information on the interaction between the incident particles and the lattice atoms. The present paper reports an experimental study of the energy spectra of secondary ions emitted on bombardment of metal targets with 7.5 – 80 keV ions.

APPARATUS AND EXPERIMENTAL TECHNIQUE

The apparatus used is shown schematically in Fig. 1. A target 1, made of molybdenum or beryllium strip 0.1 mm thick, is bombarded with monoenergetic ions of known masses, produced by a mass monochromator described earlier.[1] The target temperature is raised by a heater 2. The ion beam (10^{-8}-10^{-3} A/cm^2 density) is incident at an angle of 45° to the target surface. The energy spectra are obtained for ions emitted within a cone whose axis is perpendicular to the primary beam and has a vertex angle of 20°.

To avoid the effect of stray electric and magnetic fields the target was placed in the center of
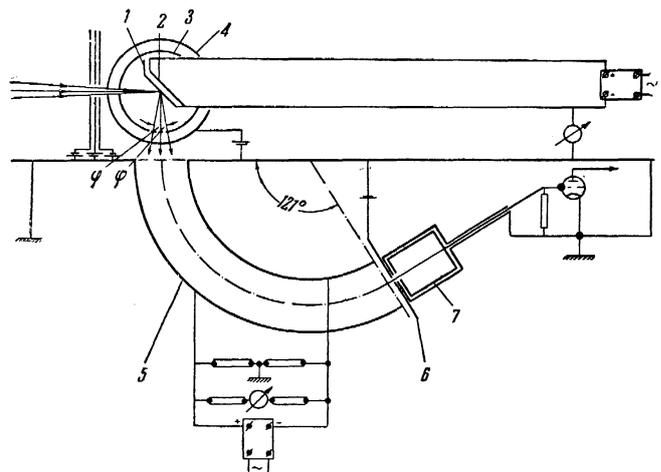

FIG. 1. Apparatus used to measure the energy distribution of secondary ions.

two concentric soft-iron spherical electrodes 3 and 4 with apertures covered by molybdenum grids of 90% penetrability. Preparation of the target for measurements was the same as described in [1]. Most of the measurements were carried out on targets heated to 1300° K and cleaned by preliminary ion bombardment.[1] The pressure of the residual gases in the measurement chamber was kept at $(1 - 3) \times 10^{-7}$ mm Hg. The energies of the secondary ions were determined with a paraboloidal electrostatic analyzer 5, designed by R. I. Sobolev
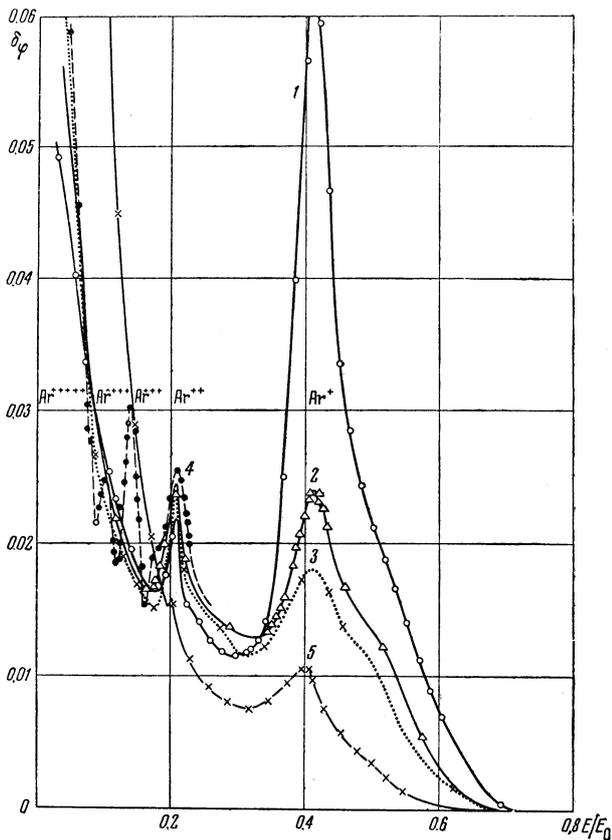
FIG. 2. Dependence of δ^{+}_{φ} on E/E_0 for Ar^{+} on Mo at various primary energies E_0: 1) 10 keV; 2) 30 keV; 3) 40 keV; 4) 80 keV; 5) 30 keV, Ar^{+} on cold Mo.

using the theory of axially symmetric focusing fields developed by Malov.[2] The principal advantage of this analyzer, compared with the Hughes-Rojansky instrument, was its ability to focus on the receiver slit 6 all the secondary ions which left the target within the specified cone; this increased the sensitivity considerably. The focusing was obtained by using curved deflecting plates.

The resolving power of the analyzer was $\Delta E/E \approx 80$. The current recorded by the ion receiver 7 was measured with an electrometer amplifier which had a sensitivity of 10^{-15} A/division. The current I_{an} was recorded on photosensitive paper by a two-coordinate galvanometer, as a function of the potential difference U_{an} between the analyzer plates. Appropriate conversion of the record gave the energy spectra of the secondary electrons in the form $\delta^{\pm}_{\varphi}$ (E) or $\delta^{\pm}_{\varphi}$ (E/E$_0$), where $\delta^{\pm}_{\varphi}$ is the ratio of the current within the cone of the vertex angle 2φ, of secondary ions (positive or negative), with energies ranging from E to (E + ΔE), to the current of primary ions with energy E_0.

The graphs show $\delta^{\pm}_{\varphi}$ as the ordinate with units 7.14×10^{-13} A/μA $\cdot$ eV. The abscissas represent secondary-ion energies in electron-volts or as fractions of the primary-ion energy.

RESULTS

Over three hundred energy spectra were obtained for secondary positive and negative ions formed on bombardment of various metal targets with the 7.5 — 80 keV ions H^{+}_1, H^{+}_2, He^{+}, C^{+}_1, N^{+}_1, N^{+}_2, O^{+}_1, O^{+}_2, CO^{+}, Ar^{+} and Ar^{2+}. A detailed analysis was made of the spectra obtained on molybdenum and beryllium targets. It was found that the energy spectra of the secondary ions depended very strongly on the experimental conditions: on the energy of the primary ions E_0, the mass of the primary ions m_1, the mass of the target atoms m_2, the pressure of the residual gases at the target, the type of these residual gases, the temperature of the target, and the cleanness of the target surface. For secondary ions with comparatively large energies ($E/E_0 > 0.1$), the $\delta^{\pm}_{\varphi}$ (E) curves could be roughly divided into three groups.

A typical representative of the first group is the energy spectrum $\delta^{\pm}_{\varphi}$ (E/E$_0$) of the positive secondary ions produced by bombardment of molybdenum with Ar^{+} ions of various energies, shown in Fig. 2; for the sake of brevity this case will be referred to as "Ar^{+} on Mo." A characteristic feature of the first group is a system of maxima clearly visible above a curve that falls continuously with increase of the secondary ion energy. Some of these maxima occurred also on the descent following a rise in the curve (Fig. 7). Figure 2 shows that with increase of the primary ion energy the secondary energies rise as well. Measured as a
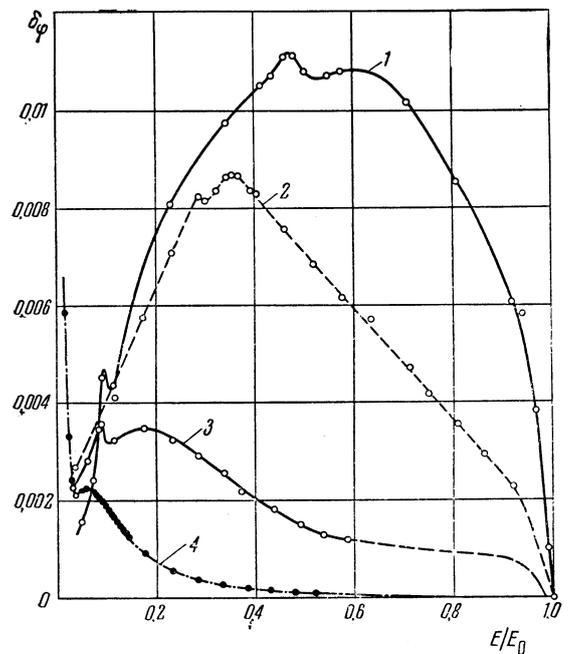

FIG. 3. The distribution δ^{+}_{φ} (E/E$_0$) for H^{+}_1 on Mo: 1) E_0 = 7.5 keV; 2) 15 keV; 3) 30 keV; 4) δ^{-}_{φ} for E_0 = 30 keV.
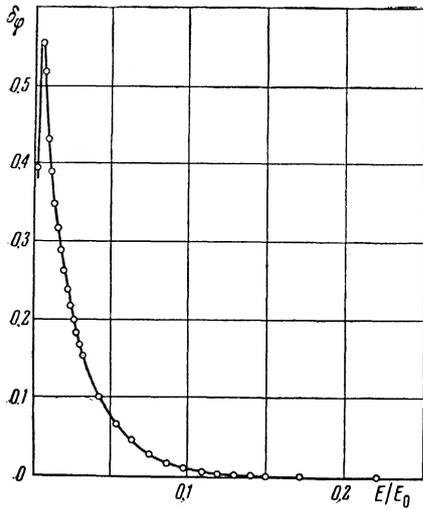
FIG. 4. The distribution δ_φ^+ (E/E$_0$) for Ar$^+$ on Be; E$_0$=80 keV.

fraction of the primary-ion energy, the abscissas X$_1$ of the first maximum on the right were found to be practically identical for all E$_0$. The numerical values of X$_1$ were different for different ratios of m$_1$/m$_2$ but they were constant for a given ratio m$_1$/m$_2$, e.g., X$_1$ = 0.41 for Ar$^+$ on Mo. The ratios of the abscissas of other maxima to X$_1$ were constant: $X_1 : X_2 : X_3 : \ldots : X_n = 1 : \frac{1}{2} : \frac{1}{3} : \ldots : \frac{1}{n}$. The number of maxima increased on increase of E$_0$; it was five for Ar$^+$ on Mo at E$_0$ = 80 keV. As E$_0$ increased the secondary-ion current at X$_1$ fell and the limiting energies of the secondary ions rose approximately proportionally to E$_0$. Adsorp-

tion of gases in the target raised the number of slow ions and reduced the number of secondary ions in the regions of X$_1$ and X$_2$. The reported dependence of the number of secondary ions on their energy was observed in all cases when m$_2$ > m$_1$ except when m$_2$/m$_1 \gtrsim$ 25.

These exceptional cases belonged to the second group of secondary-ion spectra. A typical $\delta_\varphi^\pm$ (E/E$_0$) distribution for this group is that of H$_1^+$ on Mo, given in Fig. 3. The energy spectrum is dome-like with a peak displaced toward lower energies and reduced in magnitude on increase of E$_0$. The limiting energies of the secondary ions of this group are very close to E$_0$ (E$_{\lim}$/E$_0 \approx$ 1). It was found that if the ratio of the masses of the interacting atoms was reduced the second group of energy spectra gradually approached the form of the first group. For example, when m$_2$/m$_1$ = 24 in the case of He$^+$ on Mo, a sharp peak appeared in the region E/E$_0 \approx$ 1 superimposed on the dome-like curve.

The third group included the energy spectra with m$_1$ > m$_2$. Here the number of secondary ions decreased smoothly with increase of their energy (Fig. 4). If the target surface was not clean the number of ions with small energies became greater.

Studies of the energy spectra of negative ions showed that they were somewhat different from the spectra of positive ions and that $\delta_\varphi^- < \delta_\varphi^+$ for pure targets. For example the δ_φ^- (E/E$_0$) curve for Ar$^+$ on Mo had no maxima and was similar to
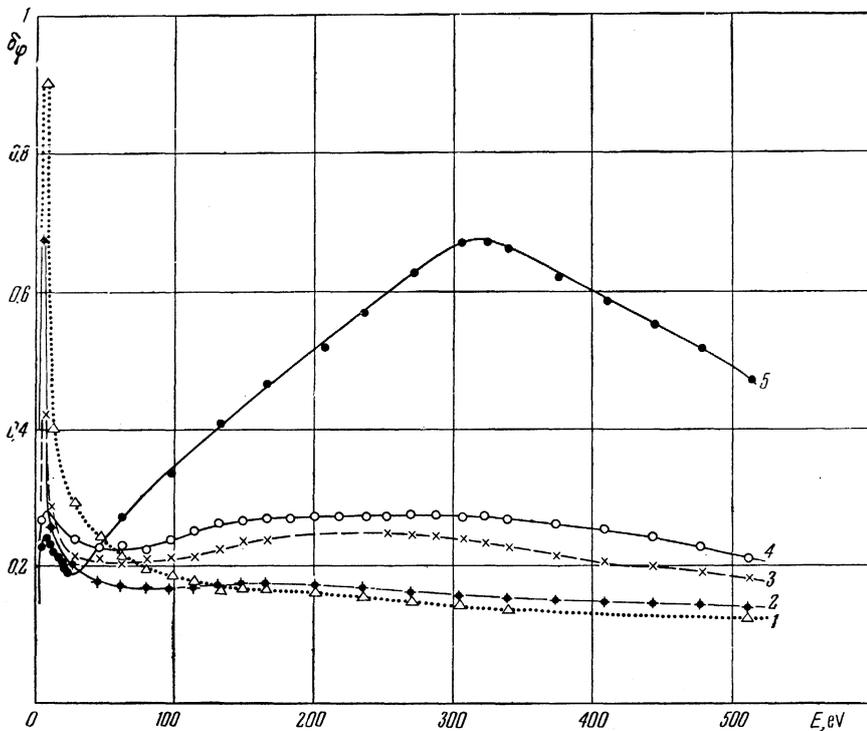

FIG. 5. The distribution δ_φ^+(E) for Ar$^+$ on Be: 1) E$_0$ = 10 keV; 2) 20 keV; 3) 30 keV; 4) 40 keV; 5) 80 keV.
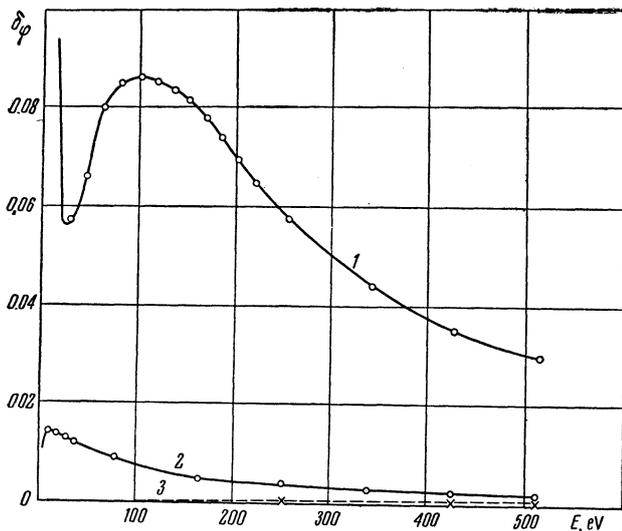
FIG. 6. The distribution δ^+_φ (E) for O^+_1 on Mo (curve 1), for He^+ on Mo (curve 2), for H^+_2 on Mo (curve 3); E_0 = 30 keV.

FIG. 7. The distribution δ^+_φ (E/E_0) for $CO^+ + N^+_2$ on Mo, E_0 = 30 keV (curve 1); the distribution δ^+_φ (E/E_0) for N^+_1 on Mo, E_0 = 22 keV (curve 2); the distribution $\delta^-_\varphi(E/E_0)$ for $CO^+ + N^+_2$ on Mo, E_0 = 30 keV (curve 3).

positive-ion spectra of the third group. In other cases when $m_1 < m_2$ some maxima were present in the case of negative ions but they were not very pronounced (curve 3 in Fig. 7).

For the slow secondary ions, the initial portions of all the energy spectra had maxima between 5 and 30 eV. The positions of these maxima did not depend on the primary-ion energy but on the target material and the state of its surface (cf. δ^+_φ (E) curves for Ar^+ on Be in Fig. 5). With increase of E_0 the magnitudes of the peaks for the positive slow ions were reduced; in the case of Ar^+ on Mo, however, the converse was observed. Contamination of the target, e.g., by cooling to room temperature at p = (1 — 3) × 10 mm Hg, produced a considerable rise of δ^+_φ and a displacement of the slow-ion peak. A cold Mo target bombarded with Ar^+ ions yielded a δ^+_φ slow-ion peak (at 30 eV) which was ten times greater than for a hot target (at 5 — 6 eV). When $m_1 \ll m_2$ (H^+_1 on Mo, Fig. 6), a clean target emitted no slow ions and the spectrum began from about 100 eV; slow ions appeared only when the target was contaminated.

A maximum was also found in the region 100 — 400 eV which increased in magnitude with increase of E_0 and with the cleanness of the target surface. Its position depended on the target material: 80 — 100 eV for O^+ on Mo (Fig. 6) and 200 — 300 eV for Ar^+ on Be (Fig. 5). In the 100 — 400 eV range the values of δ^+_φ rose with E_0 (Fig. 5) if the bombarding particle was other than hydrogen. Figure 6 indicates that δ^+_φ rose also on increase of the incident-ion mass.

When molecular ions (H^+_2, N^+_2, O^+_2) were used, the maxima and other features of the secondary-ion energy spectra were the same as for mona-
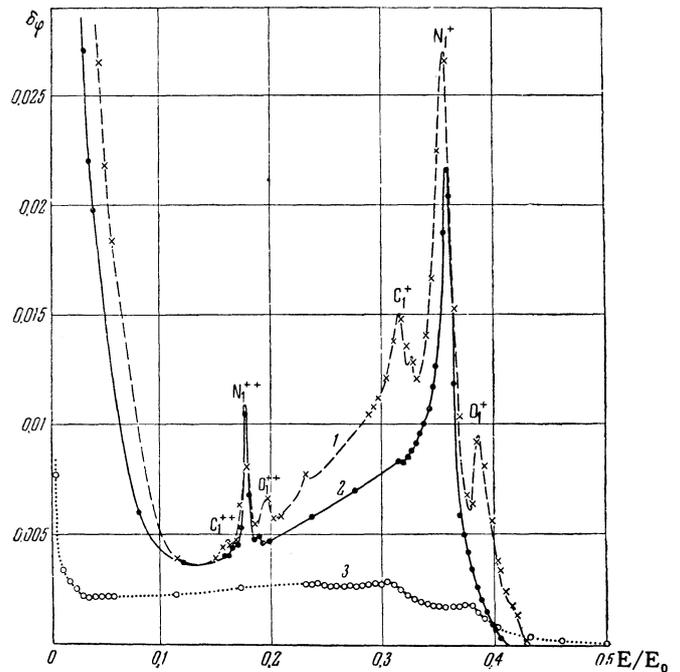
tomic primary ions of half their energy. If the molecular ion was more complex, e.g. CO^+, the secondary-ion energy spectrum was also more complex (cf. curve 2 in Fig. 2 and curve 1 in Fig. 7).

The secondary-ion energy spectra were independent of the initial charge of the bombarding ions, for example Ar^+ and Ar^{2+} gave the same results on Mo.

DISCUSSION

Many features of the observed energy spectra can be accounted for by assuming that incident atoms interact with target atoms in the same way as in the elastic scattering of free atoms. Interaction between ions and electrons (excitation and ionization) is neglected. Secondary particles consist of primary particles (m^-_1, m^0_1, m^+_1, m^{2+}_1, etc), which have experienced single or multiple collisions with lattice atoms, and of variously charged lattice atoms or surface contaminants, including primary particles captured by the lattice. The emitted lattice atoms, m^-_2, m^0_2, m^+_2, m^{2+}_2, etc obtain their energy either by collision with primary ions or by a relay mechanism involving transfer of energy between successive lattice atoms. Our discussion of charged secondary particles applies, in general, to neutral secondaries as well.
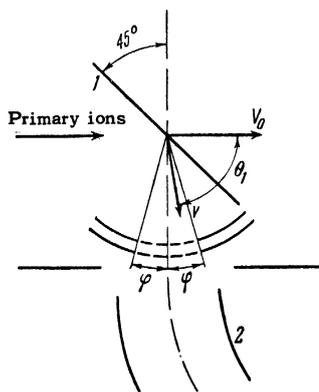
FIG. 8. A diagram for calculation of limiting energies: 1) target, 2) analyzer; V_0 is the initial velocity of primary ions, and V is the velocity of secondary ions.

To interpret the energy spectra of secondaries we must use the laws of energy and momentum conservation in collisions. The energy of a particle with mass m_1 after a collision with a particle m_2 at rest is given by

$$E_1 = E_0(1 + a)^{-2}(\cos\theta_1 \pm \sqrt{a^2 - \sin^2\theta_1})^2, \qquad (1)$$

where θ_1 is the angle of deflection of the primary particle m_1 from its initial direction of motion in the laboratory system of coordinates; $a = m_2/m_1$. It follows from Fig. 8 that in our case $(90° - \varphi)$ $\leq \theta_1 \leq (90° + \varphi)$. Therefore, the lowest and highest energies $(E_1)_{\lim}$ of the particles that enter the analyzer after single collisions with the lattice atoms are given by

$$(E_1)_{\lim} = E_0(1 + a)^{-2}(\pm\sin\varphi \pm \sqrt{a^2 - \cos^2\varphi})^2. \qquad (2)$$

Substituting $m_1 = 40$ and $m_2 = 92 - 100$ into Eq. (2) we can find the limiting energies of the Ar^+ ions scattered in the direction of the analyzer after single collisions with Mo target atoms. If these energies are expressed in relative units, taking $E_0 = 1$, we find that $0.333 \leq (E_1/E_0) \leq 0.498$ and the mean value is $\overline{E_1/E_0} = 0.41$. The abscissa of X_1 in Fig. 2 has this value of 0.41 and the greatest part of the X_1 peak lies within the limits of E_1/E_0 just specified. Similar conclusions for other combinations of masses m_1 and m_2, including H_1^+ on Be, give equally good agreement between the experimental limits of X_1 and the calculated values of $(E_2)_{\lim}/E_0$. It is therefore clear that when $m_1 < m_2$ the maxima X_1 on $\delta_\varphi^\pm(E/E_0)$ curves are due to primary ions scattered once by the target atoms. The absence of such maxima in the spectra $\delta_\varphi(E/E_0)$ for Ar on Mo and N_1^+ on Mo confirms this conclusion since argon and nitrogen atoms do not form negative ions.

If the bombarding atom has a strong affinity for electrons, maxima appear also in the negative ion spectra, for example O_1^+ on Mo (Fig. 7).

The reason for maxima at the abscissas X_1, X_2, X_3 etc, which are in the ratio of $1 : \frac{1}{2} : \frac{1}{3} : \ldots : \frac{1}{n}$,

becomes obvious when it is realized that in the transformation of the $I_{an} = f(U_{an})$ into $\delta_\varphi^\pm(E/E_0)$ all the secondary ions were taken to be singly charged. In fact these maxima represent loss of one, two, three, etc electrons in the process of scattering. Since the probability of electron loss rises with increase of the particle velocity, the number of maxima should rise with E_0 as in Fig. 2 and in similar spectra for other combinations of $m_1 < m_2$.

Substitution of the values of a and θ_1 for H_1^+ on Mo $(m_1 \ll m_2)$ into Eq. (2) shows that among the reflected ions there should be groups with energies close to E_0 $(0.975 < E_1/E_0 \leq 0.986)$. Ions with such energies are represented by the experimental curves in Fig. 3.

The third group of spectra was found only in two cases: either when $m_1 > m_2$, or when $m_1 < m_2$ if the incident atom had no great affinity for electrons. This is in full accord with our model, since in the case $m_1 > m_2$ the particle m_1 cannot be deflected by an angle greater than $\theta_{\lim} = \sin^{-1}a$. Thus the inequality $\sin^{-1}a < (\pi/2 - \varphi)$ can be used as the condition of the absence of maxima (Fig. 1).

The coincidence of the spectra of secondary ions produced by diatomic (H_2^+, O_2^+) and monatomic $(H_1^+$ and $O_1^+)$ ions when their energies are in the ratio 2/1 confirms the conclusion of many investigators that incident molecular ions are dissociated in the interaction with the target. The presence of very small numbers of ions with energies $E > 0.5E_0$ in such spectra also shows that some ions $(O_2^+$ or $H_2^+)$ are reflected without dissociation. Extension of these ideas to more complex molecules makes it possible to interpret the spectra of secondary ions produced by them (Fig. 7).

Since secondary-ion spectra extend over a wider range than that given by Eq. (2), it is necessary to consider not only single collisions but also other processes by which secondary ions can be formed. Simple calculations, similar to that just given, show that secondary particles contain groups of ions (or neutral atoms) which enter the analyzer after successive scattering from two, three or more atoms of the target (or its contaminants). The number of collisions depends on the angle of observation and on the relationships between m_1, m_2, Z_1 and Z_2, as well as on the initial energy of the incident ions. For Ar^+ on Mo, within the range of energies employed, the analyzer can receive ions which suffered not more than three collisions. On decrease of m_1 and Z_1 the number of collisions increases and in the case of H_1^+ on Mo most of the secondary ions are multiply scattered; this alters

the energy distribution curve quite considerably (Fig. 3). There is also a contribution from ions of the target material and its contaminants; this will be discussed below.

In contrast to spectra of the first and second types, particles in the spectra of the third type include practically no reflected ions at sufficiently large values of E_0. For example, in the case of Ar^+ on Be these ions can enter the analyzer only after seven collisions ($80° : 13° \approx 7$), and their energy should not exceed $0.04 E_0$ = $[(1 + a)^{-1} \cos \theta_{lim}]^{14} E_0$. However, the observed spectrum of secondary ions, shown in Fig. 4, extends up to $E > 0.2 E_0$. Consequently ions of that spectrum must be formed by ionization of the target or contaminant atoms which have received sufficient kinetic energy to eject them from the target; this kinetic energy is supplied by collisions with primary ions (including reflected ones) or with target atoms which have experienced collisions earlier.

The energy and momentum conservation laws yield the following expression for the energy E_2 transferred from an incident atom of mass m_1 to an atom of mass of m_2 at rest:

$$E_2 = 4 m_1 m_2 (m_1 + m_2)^{-2} E_0 \cos^2 \gamma_{12} = K_{12} E_0 \cos^2 \gamma_{12}, \quad (3)$$

where γ_{12} is the angle between the velocity vectors of the primary ion before collision and the secondary particle (m_2) after collision. Using a representation similar to that shown in Fig. 8, we find that $(\pi/2 - \varphi) \leq \gamma_{12} \leq \pi/2$. Consequently the energy transferred to particles that move toward the analyzer immediately after collisions with the primary ions lies between the limits

$$0 \leqslant E_2 \leqslant K_{12} E_0 \sin^2 \varphi. \quad (4)$$

It follows that under our experimental conditions we have $0 \leq E_2 \leq 0.03 E_0$ for any combination of masses m_1 and m_2. In many cases the energy E_2 is comparable with the energy necessary to displace a lattice atom E_d,[3] and these displacement energies should therefore be included in any analysis of the energy spectra of ejected particles. Brinkman[4] calculated the energy distribution for such displaced atoms. This distribution is given by the following simplified expressions

$$dn / dE = C / E^2 \text{ when } E_d < E_2 < K_{12} E_0, \quad (5)$$
$$dn / dE = 0 \quad \text{when } E_2 < E_d,$$

where n is the number of atoms displaced in all directions, and C depends on the masses and atomic numbers of the interacting particles, the number of primary ions and their energy. Of the particles represented by Eq. (5) we are interested

only in those which leave the target in the direction of the analyzer and which are ionized. The energy spectrum of such ions differs from that of Eq. (5) because the probability of electron loss rises with increase of the ejected ion velocity. The limiting energies are slightly altered. On the surface of a real target there are always atoms (target and contaminants) with different binding energies and these energies may vary with the direction of displacement. Therefore, the lower limit of the measured spectrum may be rather indefinite and the peak may not be as sharp as indicated by Eq. (5) (cf. Fig. 5). If there are few or no foreign atoms on the target, then the position of the maximum nearest to the coordinate origin of $\delta_\varphi^{\pm} (E)$ curves is governed by the binding energy of those atoms in the target surface ejected in the direction of the analyzer. On increase of E_0 the contribution of ions ejected from deeper layers of the target becomes more and more important. Consequently a second maximum appears on $\delta_\varphi^+ (E)$ curves and its position is governed by the displacement energies of atoms in the interior of the target. For O^+ on Mo (curve 1 in Fig. 6) this second maximum occurs at $80 - 100$ eV, near the energy threshold for sputtering of Mo by ions.[5] For Ar^+ on Be (Fig. 5) a similar maximum occurs at $290 - 330$ eV, indicating that the energies of displacement of beryllium atoms lie in this range.

According to Eq. (4) the energies of ions knocked out by first collisions with primary ions do not exceed $E_2 = E_0 K_{12} \sin^2 \varphi = 0.018 E_0 = 1440$ eV for 80 keV Ar^+ on Be while for 80-keV Ar^+ on Mo the limit is $0.0254 E_0 = 2000$ eV. However, Fig. 4 shows that the secondary ions included particles with energies up to $0.22 E_0$, indicating an important contribution from secondary ions formed from atoms which received their energy by the relay transfer mechanism.

The energy acquired by a particle at the n-th stage of the relay is given by

$$(E_2)_n = E_0 K_{12} \cos^2 \gamma_{12} \cdot K_{23} \cos^2 \gamma_{23} \ldots K_{n, n+1} \cos^2 \gamma_{n, n+1}, \quad (6)$$

where $K_{n, n+1} = 4 m_n m_{n+1} / (m_n + m_{n+1})^2$; $\gamma_{n, n+1}$ is the angle between the vectors of the pre-collision velocity of atoms with mass m_n and the post-collision velocity of particles with mass m_{n+1}. The expression (6) is valid if the distance between atoms m_2 and m_{n+1} before collision is small compared with the distance between the target and the analyzer (the situation can be represented schematically as in Fig. 8). In order to be registered by the analyzer the displaced atom m_{n+1} should be ionized, the sum of the deflection angles γ should satisfy

$$\pi/2 - \varphi \leqslant (\gamma_{12} + \gamma_{23} + \ldots + \gamma_{n, n+1}) \leqslant \pi/2 + \varphi, \quad (7)$$

and the energy transferred at each relay stage should exceed E_d. An analysis of Eq. (6) and of these conditions indicates that the energy of the secondary ions received by the analyzer lies within the range

$$0 \leqslant (E_2)_n < E_0 K_{12} K_{23} \ldots K_{n, n+1} \cos^{2n}\left(\frac{\pi - 2\varphi}{n}\right). \quad (8)$$

Substitution of the values of K_{12}, K_{23}, . . ., $K_{n, n+1}$, φ and n into Eq. (8) and comparison of the result with Fig. 4 shows that the third and further stages of the relay energy transfer do not contribute materially to emission. The limiting value of the energy transferable to target atoms which are subsequently ejected can be found by assuming that the relay energy transfer chain is infinite ($n \rightarrow \infty$, $\gamma_i \rightarrow 0$, $(E_2)_{lim} = K_{12} E_0$), and that $K_{23} = K_{34} = \ldots = K_{n, n+1} = 1$, since $m_2 = m_3 = \ldots = m_{n+1}$. The probability of ejection of such ions is extremely small and, therefore, the actual energies of the emitted atoms are considerably smaller than $(E_2)_{lim}$. This conclusion is confirmed by the results of Stanton,[6] published after the present paper was finished.

Our analysis shows that the energy of Mo ions or atoms ejected by H_1^+ ions in the direction of the analyzer should not exceed $0.0425 E_0$. This confirms the suggestion that most secondary ions represented by the spectrum in Fig. 3 were produced by multiple collisions. This suggestion is valid only for clean targets. If the target surface is contaminated with atoms lighter than Mo, for example by carbon, then some of the ejected Mo atoms can acquire greater energies because

$$(E_2)_{lim} = K_{H, C} K_{C, Mo} E_0 = 0.284 \cdot 0.408 E_0 = 0.116 E_0.$$

This model accounts also for the absence of slow ($0 - 100$ eV) secondary ions on bombardment of clean molybdenum targets with H_2^+ ions of 30 keV energy (Fig. 6). A 30-keV H_2^+ ion can accelerate directly an Mo atom toward the analyzer by giving it an energy not greater than 19.3 eV; this follows from Eq. (3) if dissociation of H_2^+ is allowed for. Since the energy of displacement of the Mo atoms is roughly equal to 100 eV, a single collision with H_1^+ cannot direct an ejected Mo atom toward the analyzer. In the second stage of the energy relay process Mo atoms can

obtain energies up to 180 eV but only those with energies greater than $E_d \approx 100$ eV can leave the target because most of these atoms are below the uppermost surface layer of the target.

CONCLUSIONS

The results obtained have confirmed satisfactorily the interaction model suggested by many workers, that atomic particles of medium energies ($1 - 100$ keV) collide with atoms in the solid practically as if the latter were free particles.

Calculations of the energy limits of various components of secondary ion emission have explained some details of the emission mechanism. They have also accounted for many features of the energy spectra of secondary particles reported here and by other workers investigating secondary ion emission, sputtering, radiation effects and gas evolution from surfaces bombarded with atoms or ions. For example, the suggestion of several workers that most molecular ions are dissociated on impact with a target surface has been fully confirmed. It has been found for the first time that ions reflected from the target are further "stripped." An earlier suggestion that secondary ion emission is independent of the initial charge of the bombarding ion has also been confirmed.

[1] B. V. Panin, JETP 41, 3 (1961), Soviet Phys. JETP 14, 1 (1962).

[2] A. F. Malov, Nekotorye voprosy éksperimental'noĭ fiziki (Some Problems of Experimental Physics), No. 2, Atomizdat, M. 1959.

[3] F. Seitz and D. Turnbull, Solid State Physics, Vol. 7, Academic Press, New York and London, 1958.

[4] J. A. Brinkman, Am. J. Phys. 24, 246 (1956).

[5] G. K. Wehner, Advances in Electronics and Electron Physics 7, 239 (1955).

[6] H. E. Stanton, J. Appl. Phys. 31, 678 (1960).